INFLUÊNCIA DO TIPO DE OXIDANTE NA COMBUSTÃO DE COMBUSTÍVEL LÍQUIDO EM UM FORNO DE ALUMÍNIO

Aluno: Rafael Cezar Menezes
Orientador: Angela O. Nieckele

Introduction

There are several industrial combustion applications which may benefit from the use of oxygen-enriched air or pure oxygen as the oxidizer during the combustion process. The effects are many. Oxygen enrichment increases the flame temperature, promotes soot formation and oxidation, and can decrease pollutant emissions compared with hydrocarbon-air systems.

The formation of nitrogen oxides (NOx) in air-feed combustion systems represents a significant source for this pollutant within the industrial sector. With the increase in the world-wide utilization of fossil fuels, the control of NOx emissions has become an issue of global concern. Additionally, with increasing oil prices, the use of lower quality fuels will worsen the problem. Advances in computational modeling tools and the increased performance of computers have made comprehensive modeling of NOx formation and destruction a valuable tool to provide insights and understanding of the NOx reaction processes in combustion systems. This technology has the potential to enhance the application of various combustion techniques used to reduce NOx emissions from practical combustion systems (Hill and Smmot, 2000).

Hill and Smoot (2000) presented a review on the modeling of NOx reactions in combustion systems, with an emphasis on coal-fired systems, including NOx control technologies, NOx reaction processes, and techniques to calculate chemical kinetics in turbulent flames. Models of NOx formation in combustion systems were reviewed. Comparisons of measured and predicted values of NOx concentrations were presented for several full-scale and laboratory-scale systems.

Numerical modeling has became an important tool in the design and optimization of industrial equipments and also in the prediction of the emission of pollutants such as CO (carbon monoxide), SOx (sulfur oxides), and NOx. Recently, several numerical studies were developed to analyze the combustion process with different fuels, using pure air, oxygen or a mixture of both as the oxidizer. These studies provided detailed descriptions for the temperature, velocity and species concentration fields within various geometries of industrial combustion equipment.

The work of Yang and Blasiak (2005) described the CFD modeling of the combustion of liquified propane gas (LPG) with highly preheated air in a regenerative burner system. Results for various parameters, including the furnace-wall temperature and the concentration of gaseous species, were obtained for a semi-industrial furnace. The results indicated that the flame spread could be well predicted by using the numerical model. It was also found that the regenerative burner could provide high energy savings and lower emissions of NO.

In Frassoldati et al. (2005), the attention was focused on a new procedure, based on CFD, for the determination of NOx emissions from combustion processes, which allowed the use of very detailed reaction schemes. The procedure was validated for the case of high swirled confined natural gas diffusion flames, with available experimental data of German TECFLAM (2006) for a 150 kW thermal load swirl burner. The predictions of NOx were obtained by post-processing the flow and temperature fields, as predicted by the CFD model,

and lumping together computational cells similar in terms of NOx formation. The resulting macro-cells were assumed to be a network of ideal reactors, which were simulated adopting detailed kinetic mechanisms.

Wang at al. (2005) developed a comprehensive CFD model by integrating procedures for detailed chemistry, soot formation and oxidation, and thermal radiation, into a three-dimensional unstructured CFD code. The detailed chemistry kinetics was modeled by using 122 chemical species and 677 elementary reactions. The model was applied to an oxygen-enriched, turbulent, non-premixed propane flame. The results showed that soot radiation decreased flame temperature and NOx emissions, substantially, especially in the flame-tip region. They also investigated the importance of modeling the radiation effects accurately for predicting the soot and NOx formation adequately.

Nieckele et al. (2004) described a numerical simulation of the 100% oxy-firing combustion process inside an industrial aluminum re-melting reverb furnace. Three different configurations were analyzed including the comparison between the staged versus non-staged combustion processes. The numerical procedure was based on the finite volume formulation and the kappa-epsilon model of turbulence. The combustion was modeled based on the finite rate models of Arrhenius and Magnussen, and the Discrete Transfer Radiation model was employed for predicting the radiation heat transfer. The numerical predictions allowed for the determination of the flame patterns, species concentration distribution, temperature and velocity fields.

The flow field inside aluminum furnaces with different types of burners and operating conditions was analyzed in (Nieckele et al, 2004, 2005). Also, numerical and experimental investigation in an industrial aluminum melting furnace with oxygen enriched combustion was carried out in Brewster et al. (2001). The temperature distribution on the refractory walls was verified. The model over estimated the turbulent mixture and, on the other hand, the CO (carbon monoxide) concentrations were under estimated near the burner region, probably because the kinetic effects were neglected. Numerical simulations inside an industrial burner in an aluminum melting furnace were also carried out in Mukhopadhyay et al. 2001. It was shown that the flame height grows with the fuel velocity for a given air-fuel ratio, and with the reduction of the air velocity, for a given fuel velocity. In Nieckele et al. (2002) a turbulent natural gas flame in a cylindrical furnace was simulated, using finite rate models and modeling chemical reactions in two different ways: in a simple manner, where the fuel combustion was predicted in one single global reaction; and with a two-step process, where the carbon monoxide could be predicted in an intermediate reaction. The results for both models showed a good agreement with the experimental data found in the literature, although it was observed that the physical phenomena was better described by the two step reaction.

With respect to the numerical modeling of the spray flow of liquid fuels, a single model that predicted the source terms for the mean mixture fraction and its variance is proposed in Reveillon and Vervisch, (2000). The source term for the mean mixture fraction due to the droplet vaporization is normally provided by an Eulerian-Lagrangean formulation which, according to the authors, is not satisfactory when applied to the calculation of the source terms that are associated to the fluctuations of the mixture fraction. In Demoulin and Borghi (2002) turbulent combustion of a diesel spray was investigated, utilizing probability density functions for each fluctuating variable in the liquid and gas phases, showed that a proper description of the temperature fluctuations caused by the presence of the droplets is crucial for a better estimation of the reaction rates.

In the present work, numerical simulations were carried out using the commercial package FLUENT, version 6.2 (2006) to determine the flow field, species and temperature distribution inside an aluminum industrial furnace, employing air and pure oxygen for the combustion of liquid fuel. The advantages and disadvantages of each type of oxidant are addressed.

Problem Set-up

The furnace geometry was represented as a rectangular prism of 4.0 m length, 1.5 m wide and 2.0 m height, presented in Fig. 1a. Fig. 1b illustrates details of the frontal plane, and different view of the inlet configuration. Due to symmetry, only half furnace was solved.

The lower limit of the furnace was considered to be the liquid aluminum surface with a small aluminum oxide layer of 0.5 mm above it. The aluminum oxide layer was considered to describe the oxidization of the aluminum surface by the water that results from the combustion, which can act as an isolator and can compromise the quality of the product.

The vertical symmetry plane passes through the center of the chimney between the two pairs of oxidant and fuel injectors. The inlets of oxidant and fuel as well as the outlet of the combustion products are located at the same wall (Fig. 1b). The center of the burner is located 0.65m above the aluminum oxide layer and 0.80m away from the symmetry plane. Fuel is injected in the center and the oxidant surrounds it. The oxidant injector is located 0.20m above the burner. Both burner and oxidant lance are formed by a central opening and a set of small orifices surrounding the central opening, which are here represented by an annular opening. Two cases were analyzed, both with liquid fuel $C_{19}H_{30}$, one with oxygen as oxidant and the other with air as oxidant. The inlet geometry of oxidant depends on the oxidant. The liquid fuel burner has a central opening area equal to 2.89×10^{-4} m^2 for both cases. For the case with oxygen as oxidant, the oxidant and burner lances have the same geometry, and the annular opening area is equal to 1.38×10^{-3} m^2. For the case with air as oxidant, a larger mass flow rate is necessary. Therefore, the inlet areas are larger to maintain the same order of magnitude of the velocity at the entrance. In this case, in the oxidant lance the central opening area is equal to 2.13×10^{-3} m^2. The annular opening areas for both lances are equal to 3.53×10^{-3} m^2. The jets are directed away from the refractory walls, angles of 15° in the vertical plane and 10° in the horizontal plane were set. The height of the center of the rectangular chimney coincides with that for center of the burner, its half width measures 0.50m and its height measures 0.60m.
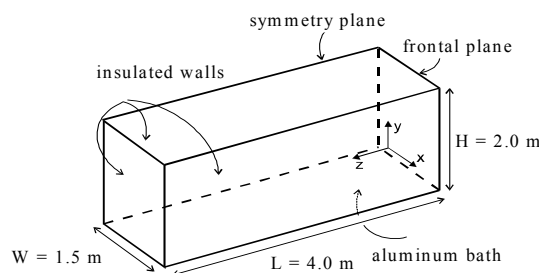
(a) Schematic of the furnace and geometry
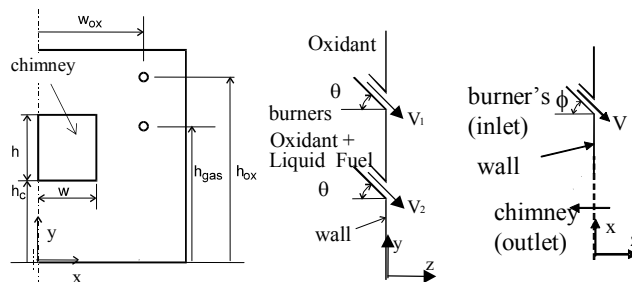
(b) Injection and chimney geometry

Figure 1. Problem configuration

Considering a typical aluminum load of 16 tons (which corresponds to a volume of $6m^3$), assuming an approximate process time of 1 hour, and knowing that the aluminum latent heat is 397.4 kJ/kg, a heat transfer rate of 880 kW must be extracted from the aluminum surface, in order to represent the energy necessary to melt the entire load of aluminum.

The inlet temperatures of oxygen and air were set as 298 K, while all refractory walls were considered as insulated. The inferior surface of the furnace represented the aluminum bath; and the aluminum melting temperature of 1013 K was imposed.

Mathematical Modeling

The turbulent flow and heat transfer inside the furnace were solved numerically using the finite volume technique and the commercial code FLUENT, version 6.2. The average forms of the conservation equations of mass and momentum are given by:

$$\mathbf{div}\,(\rho\mathbf{v}) = 0 \qquad ; \qquad div(\rho\mathbf{vv}) = div[\mu_{ef}\,(grad\,\mathbf{v} + (grad\,\mathbf{v})^T\,] - grad\,P \qquad (1)$$

where ρ is the density, $\mathbf{v}$ is the velocity vector, and $\mu_{ef} = \mu + \mu_t$ is the effective viscosity, obtained by the Boussinesq's hypothesis. The modified total pressure $P = p - (2/3)\,[\,\mu_{ef}\,\mathbf{div}\,\mathbf{v} + \rho\,\kappa\,]$, takes into account the contributions due to the turbulent fluctuations. The turbulence $\kappa-\varepsilon$ model was used for calculating the turbulent viscosity, which is defined as $\mu_t = c_\mu\,\rho\,\kappa^2/\varepsilon$, where κ is the turbulent kinetic energy and ε the dissipation for the turbulence kinetic energy. The conservation equations of κ and ε are given by:

$$\mathbf{div}\,(\rho\mathbf{v}\kappa) = \mathbf{div}\big[(\mu + \mu_t / Pr_\kappa)\,\mathbf{grad}\,\kappa\big] + (G - \rho\varepsilon)\ ; \qquad (2)$$

$$\mathbf{div}\,(\rho\mathbf{v}\varepsilon) = \mathbf{div}\left[(\mu + \frac{\mu_t}{Pr_\varepsilon})\,\mathbf{grad}\,\varepsilon\right] + (c_1 G - c_2 \rho\varepsilon)\,\frac{\varepsilon}{\kappa} \qquad (3)$$

In the above equations, Pr_κ and Pr_ε are the turbulent Prandtl numbers for κ and ε, and were set equal to 0.7. The constants were set as $c_1 = 1.4$, $c_2 = 1.9$, and $c_\mu = 0.09$. The term $G = \mu_t\,[\mathbf{grad}\,\mathbf{v} + (\mathbf{grad}\,\mathbf{v})^T]\,o\,\mathbf{grad}\,\mathbf{v}$ stands for the generation of turbulence kinetic energy. The above equations were solved simultaneously with the conservation equations of mass and momentum, providing the solution for the turbulent flow problem.

The density of the gaseous mixture was calculated using the ideal gas law, $\rho = p_{op} / [RT\Sigma_i (m_i/M_i)]$, where p_{op} is the average operation pressure inside the furnace, that was to be equal to one atmosphere.

For all dependent variables wall functions were employed for setting up the conditions close to the solid boundaries, following the procedure described in Launder and Spalding (1974) and Patankar and Spalding, 1967.

The temperature field within the furnace was obtained solving the energy equation, where the total enthalpy h is defined by the sum of the enthalpies for each species h_i weighted by its mass fraction m_i,

$$\mathbf{div}(\rho\,\mathbf{v}\,h) = \mathbf{div}\left[\left(\frac{\mu}{Pr} + \frac{\mu_t}{Pr_t}\right)\mathbf{grad}\,h\right] + S_h\ ; \quad h = \Sigma_i\,m_i\,h_i\ ; \quad h_i = \int_{T_{ref,j}}^{T} cp_j\,dT + h_j^o(T_{ref,j}). \qquad (4)$$

and h_i^o is the formation enthalpy at the reference temperature $T_{ref,j}$ and cp_j is the specific heat at constant pressure of specie j. The term $S_h = S_{reac} + S_{rad}$, represents the enthalpy source due to the chemical reactions (combustion) and the radiation heat transfer. The turbulent Prandtl number, Pr_t, was set at 0.5.

Auxiliary Models

The source term in the energy equation due to radiation was calculated using the Discrete Transfer Radiation Model (DTRM). In this model, the change in the radiant intensity I, integrated over all wavelengths, along a path S is calculated according to $dI/dS = -\alpha I + \alpha \sigma T^4/\pi$, if scattering is neglected. The terms on the left side represent the loss by absorption and the gain by emission due to the participating medium, respectively.

The model integrates the above expression along several directions starting from each control volume on the domain surfaces. The source term S_{rad} is calculated locally by summing the changes in intensity for all the rays crossing the control volume. The Weighted Sum of Gray Gases Model (WSGGM) was used for the calculation of the absorption coefficient (Smith et al, 1982).

The generalized finite rate model, combined with the Arrhenius-Magnussen model (Fluent, 2006; Kuo, 1986), was selected to obtain the source term due to chemical reactions in the energy equation. The chemical species distributions are obtained through the solution of n-1 transport conservation equations, where n represents the number of species. The general form of the conservation equation for each chemical species is given by

$$\mathbf{div}\left(\rho\,\mathbf{v}\,m_i\right) = \mathbf{div}\left[\left(\mu/Sc + \mu_t/Sc_t\right)\mathbf{grad}\,m_i\right] + R_i + S_i \tag{5}$$

In the above equation, the terms R_i and S_i represent the sources for each species. The former is associated with the transformations due to chemical reactions, and the later may represent addition from the dispersed phase. The term R_i, may be expressed by the sum of the reaction rates (generation or consumption) for species i in every reaction k, as denoted by $R_{i,k}$, according to $R_i = \Sigma_k R_{i,k}$. The turbulent effect is taken in consideration by the turbulent diffusion coefficient, μ_t/Sc_t, where the turbulent Schmidt number Sc_t was set equal to 0.5.

With the combined Arrhenius-Magnussen model, the combustion reactions rates are determined by the smallest value between the Arrhenius and the Magnussen models, which are respectively given by

$$R_{i,k} = \eta_{i,k} M_i T^{\beta_k} A_k \exp\left(-E_k/RT\right)\prod_j C_j^{\gamma_{j,k}} \quad ; \quad R_{i,k} = \eta_{i,k} M_i K_1 \rho \frac{\varepsilon}{k}\,\mathbf{min}\left[\frac{m_{j*}}{\eta_{j*,k}M_{j*}}; K_2 \frac{\Sigma_p m_p}{\Sigma_p \eta_{p,k} M_p}\right] \tag{6}$$

In these expressions j* represents the reactant which gives the smallest value for $R_{i,k}$, and K_1 and K_2 are empirical constants, set as 4.0 and 0.5, respectively.

Two cases were considered, in the first one, pure oxygen was employed as oxidant while for the second case, air was used as oxidant. For both cases, liquid fuel, $C_{19}H_{30}$, was employed as fuel. The stoichiometric coefficients for the reaction must be specified in accordance to

$$C_{19}H_{30} + 26.5\,O_2 \rightarrow 19\,CO_2 + 15\,H_2O \tag{7}$$

The Magnussen reaction rate expression does not require any additional information. The parameters for Arrhenius and Arrhenius-Magnussen models are: $A_k = 3.60 \times 10^9$ (m^3/s)/kmol; $E_k = 126$ MJ/kmol; $\gamma_{O2}=1.5$, $\gamma_{CO2}=\gamma_{H2O}=\beta_k=0$.

The prediction of the trajectory of a discrete phase droplet is performed by integrating the force balance on the droplet, which is written in a Lagrangian reference frame as follows:

$$\frac{d\,u_p}{d\,t} = F_d\,(u - u_p) \quad ; \quad F_d = \frac{18\,\mu}{(\rho_p\,d_p^2)}\,C_D\,\frac{Re_d}{24} \quad ; \quad Re_d = \rho\,d_p\left|u_p - u\right|/\mu \tag{8}$$

where F_d is the drag force per unit particle mass and $\mathbf{Re}_d$ is the relative Reynolds number, u and u_p are the fluid phase and particle velocities, and d_p is the particle diameter. C_D is the drag coefficient, which depends on $\mathbf{Re}_d$

As the trajectory of a particle is computed, the droplet stream variation of heat, momentum and mass are incorporated in the subsequent continuous phase calculations. By doing so, the interphase exchange is alternately computed, considering the droplets trajectories and the conservation equation for the gaseous mixture, until the solutions in both phases stop to change.

There are basically two mechanisms that control the droplets evaporation, depending on its temperature level, T_p. If the temperature is higher then T_{bp} (boiling point) the boiling process is convective, and no longer controlled by the diffusion of molecules on the droplets surface to the continuous phase and the fuel vapor pressure. Therefore, for $T_p < T_{bp}$, the vapor molar flux is $N_i = k_c (C_{i,s} - C_{i,\infty})$, where N_i is, k_c is the mass transfer coefficient, $C_{i,s}$ and C_i, are the concentrations on the droplets surface and in the gaseous phase, respectively. For $T_p \geq T_{bp}$:

$$\frac{dd_p}{dt} = \frac{4k_\infty}{\rho_p c_{p,\infty} d_p}(1 + 0.23\sqrt{\mathbf{Re}_d}\,)\ln\left[1 + \frac{c_{p,\infty}(T_\infty - T_p)}{h_{fg}}\right] \tag{9}$$

where $c_{p,\infty}$, k_∞ and T_∞ are, respectively, the specific heat at constant pressure, thermal conductivity and gas temperature, and $h_{f,g}$ is the latent heat of volatiles involved.

The coupling between the discrete and continuous phases appears as source terms in the momentum, energy and mass equations for the continuous phase. The drag force acting on the droplet in axial direction depends on the mass flow rate of the droplet, $\dot{m}_p$. It is integrated in time with a time step Δt.

$$F = \sum F_d (u_p - u)\,\dot{m}_p\,\Delta t \tag{10}$$

Neglecting the presence of superficial combustion, the energy exchange between phases is calculated by:

$$Q = \left[\frac{\overline{m}_p}{m_{p,o}}c_p\Delta T_p + \frac{\Delta m_p}{m_{p,o}}\left(-h_{f,g} + h_{pyrol} + \int_{T_{ref}}^{T_p} c_{p,i}\,dt\right)\right]\dot{m}_{p,o} \tag{11}$$

where $\overline{m}_p$ is the average mass of the droplet in the control volume, $m_{p,o}$ and c_p are the initial mass and specific heat of the droplet, ΔT_p and Δm_p are temperature and mass variation as the droplet passes through the control volume, $h_{f,g}$ is the latent heat of the volatiles involved, h_{pyrol} and $c_{o,i}$ are the heat of pyrolisis and specific heat of theses volatiles, T_p is the droplet temperature on the control volume exit, T_{ref} is the enthalpy reference temperature.

The mass transfer to the continuous phase is calculated by examining the mass change of the droplet as it passes through each control volume: $M = (\Delta m_p / m_{p,o})\,\dot{m}_{p,o}$.

The NOx concentration is predicted using FLUENT NOx postprocessor (Fluent, 2006). Since NOx reaction rates are slow, they are not treated using an equilibrium assumption, as it was performed with the others intermediate and product species. The NOx species can be excluded from the equilibrium calculation because they are present in low concentrations and have little impact on density, temperature and other species concentration.

Thermal NOx formation is calculated by using the extended Zeldovich mechanism,

developed by Zeldovich in 1946 and described in Tomeczek and Gradon (1997). The reaction rates were obtained from the evaluation of Hanson and Salimian (1984). The presence of a second mechanism for creating NO during the combustion process was first identified by Fenimore (1971) and was denominated by "prompt NO". The prompt NO mechanism is more important in rich flames. In the present NOx prompt model, it was used a global kinetic parameter and a procedure developed by De Soete (1975).

The NOx emissions are predicted by solving a transport equation for nitric oxide (NO) concentration, using a given flow, temperature and species field. In this work only the thermal and prompt mechanisms for NOx formation were considered. Therefore, only the NO species transport equation has to be solved:

$$\mathbf{div}(\rho\,\mathbf{v}\,m_{NO}) = \mathbf{div}(\rho\,D\,\mathbf{grad}\,m_{NO}) + S_{NO} \quad ; \quad S_{NO} = M_{w,NO}\frac{d[NO]}{dt} \tag{12}$$

where S_{NO} is the source term, $M_{w,NO}$ is the molecular weight of NO (kg/gmol), and $d[NO]/dt$ is the NO formation rate for each case (Fluent, 2006).

For thermal NOx mechanism, neglecting the OH concentration, the principal reactions are:

$$O + N_2 \leftrightarrow N + NO \quad ; \quad N + O_2 \leftrightarrow O + NO \tag{13}$$
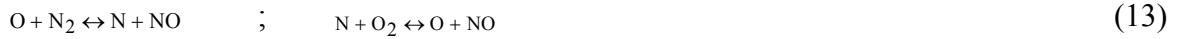
Assuming a quasi-steady state, the NO formation rate is given by:

$$\frac{d[NO]}{dt} = 2\,k_{f,1}\,[O][N_2]\frac{\left(1 - \dfrac{k_{r,1}\,k_{r,2}\,[NO]^2}{k_{f,1}\,[N_2]k_{f,2}\,[O_2]}\right)}{\left(1 + \dfrac{k_{r,1}\,[NO]}{k_{f,2}\,[O_2]}\right)} \tag{14}$$
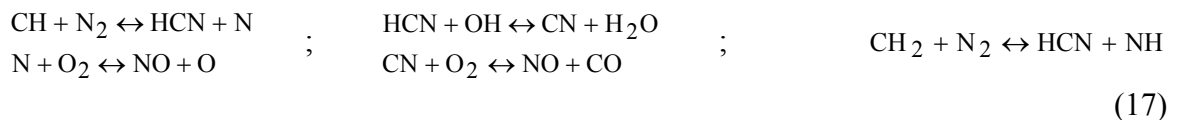
where [O], [NO], [O2], and [N2] are the concentration of [i] atoms, and $k_{i,j}$ are empirical constants (Hanson and Salimian, 1984), given by:

$$k_{f,1} = 1.8\times10^8 e^{-38370/T} \quad ; \quad k_{f,2} = 1.8\times10^4 e^{-4680/T} \quad ; \quad k_{r,1} = 3.8\times10^7 e^{-425/T} \quad ; \quad k_{r,2} = 3.81\times10^3 Te^{-20820/T} \tag{15}$$

The equilibrium approach was employed as suggested by Zeldovich (Tomeczek and Gradón, 1997). Therefore, the thermal NOx formation mechanism can be decoupled from the main combustion process, and the NOx formation rate is calculated by assuming equilibrium of the combustion reaction. The concentration of the oxygen-atom is given by:

$$[O] = 3.97\times10^5 T^{-1/2}[O_2]^{1/2}e^{-31090/T} \quad gmol/m^3 \tag{16}$$

For the prompt NOx mechanism, the reactions are:

$$\begin{aligned} CH + N_2 &\leftrightarrow HCN + N \\ N + O_2 &\leftrightarrow NO + O \end{aligned} \quad ; \quad \begin{aligned} HCN + OH &\leftrightarrow CN + H_2O \\ CN + O_2 &\leftrightarrow NO + CO \end{aligned} \quad ; \quad CH_2 + N_2 \leftrightarrow HCN + NH \tag{17}$$

For hydrocarbon fuels, the NO formation rate may be calculated by:

$$\frac{d[NO]}{dt} = f\,k'_{pr}[O_2]^a[N_2][FUEL]e^{-E'_a/RT} \tag{18}$$

where $f = 4.75 + 0.0819\ n - 23.2\ \varphi + 32\ \varphi^2 - 12.2\ \varphi^3$, $k'_{pr} = 6.4 \times 10^6 (RT/p)^{a+1}$ and $E'_a = 303474.125$ J/gmol. n is the number of carbon atoms per molecule for the hydrocarbon fuel, φ is the equivalence ratio, a is the oxygen reaction order, which depends on the flame conditions. For $N_{O_2} \geq 4.1 \times 10^{-3}$, a is equal to one and above 0.03 it is zero, else

$$a = \begin{cases} -3.95 - 0.9\ \mathbf{ln}\ N_{O_2} & ; \quad 4.1 \times 10^{-3} \leq N_{O_2} \leq 1.11 \times 10^{-2} \\ -0.35 - 0.1\ \mathbf{ln}\ N_{O_2} & ; \quad 1.11 \times 10^{-2} \leq N_{O_2} \leq 0.03 \end{cases} \qquad (19)$$

Since the flow under analysis is turbulent, temperature and composition fluctuations are taken into account by considering probability density functions. In FLUENT NOx model, a single- or joint-variable PDF in terms of a combination of a normalized temperature and species mass fraction, is used to predict the NOx emission. The mean turbulent rate of production of NO, $\overline{S}_{NO}$, is given by:

$$\overline{S}_{NO} = \int ... \int S_{NO}\ (V_1, V_2, ...)\ P\ (V_1, V_2, ...)\ dV_1\ dV_2 ... \qquad (20)$$

where V_1, V_2, ... are temperature and species concentrations, P is the probability density function, and S_{NO} is the instantaneous rate of production, given by eq. (11). This equation must be integrated at every node and at every iteration.

Results

The flow field inside the furnace was numerically obtained for the two types of oxidant. The solution was considered converged when the sum of the normalised residuals of all equations was less than 10^{-4} and the normalised enthalpy residual was less than 10^{-6}.

The mesh distribution was generated with the FLUENT auxiliary tool GAMBIT (Fluent, 2005). A grid test was performed, by doubling and by reducing in 50% the number of points in each direction. The overall agreement was very good, and the mesh was considered satisfactory for a maximum temperature difference smaller than 3%. After the grid test, an approximately uniform mesh of 134,400 control volumes, with $60 \times 40 \times 56$ elements in the x, y, and z directions, respectively, was selected. The smallest grid size was equal to 2 mm.

The absolute viscosity of the liquid fuel was $\mu = 1.72 \times 10^{-5}$ Pa s, while the thermal conductivity was $k = 0.0454$ W/(m K) for $C_{19}H_{30}$. The diffusion coefficient of all species in all mixtures was equal to the N_2 diffusion coefficient, 2.88×10^{-5} m^2/s. The mixtures specific heats were obtained by a weighted mass fraction average. Table 1 presents the composition, the molecular weight M, formation enthalpy h^o and the specific heat at constant pressure cp of fuel and oxidants (Kuo, 1986).

To model the liquid oil spray concerning the liquid fuel problem, 15 particle streams were defined into the fuel inlet region, defining a cone with angle of 45°. The droplets flow is defined from initial conditions related to the injection points of the discrete phase in the gaseous mixture. These conditions will be used as the starting point for the integration of the droplets equation of motion and calculation of their trajectories. Since the surface combustion of the particle is not being modeled, the droplets must vaporize to react with the gaseous phase. Therefore, the inlet temperature of the droplets influences the point where the combustion reaction will start. The vaporization temperature was defined as 400K, lower than the temperature at which the droplets enter the domain (495 K), indicating that vaporization starts immediately after they enter the furnace, that is, no inert heating occurs. The vaporization temperature (T_{vap}) is an arbitrary modeling constant used to define the onset of

the droplet vaporization process. The boiling temperature (T_{bp}) corresponds to the saturation temperature at atmospheric pressure for the fuel, which is the operation pressure of the furnace. In the case of $C_{19}H_{30}$, this temperature corresponds to $T_{bp}=598$ K. Unless the particle temperature has reached the boiling point, the vaporization is controlled by the fuel vapor pressure (defined as 1329 Pa) and by the diffusion coefficient for the fuel in the surrounding gas (3.79×10^{-6} m^2/s). For simplicity, constant values were assumed for the vapor pressure and the fuel diffusion coefficients during the vaporization process of the droplet. When the droplet temperature reaches the boiling point, a boiling rate equation is applied (Fluent, 2006). The latent heat of the fuel is   124 k J/kg at the atmospheric pressure. The density, specific heat capacity and thermal conductivity of the liquid fuel were defined as 960 kg/m^3, cp=1880 J/(kg K) and k= 0.12 W/(mK), respectively, and the fuel was considered as 100% volatile.

Table 1: Species properties

	Species	**% m_i**	**M_i**	**h_i^o kJ/kg**	**cp_i J/(kg K)**
Liquid Fuel	$C_{19}H_{30}$	100	258	-640,000	1000
Oxygen	O_2	100	32	0.0	1140
Air	O_2	23	32	0.0	1140
	N_2	77	28	0.0	1242
water	H_2O	0	18	-241,837	2615
carbon dioxide	CO_2	0	44	-393,532	1324

Initially pure oxygen was selected as oxidant. To accomplish the fusion of 16 tons of aluminum in one hour, a nominal thermal power equal to 1.2 MW per burner was specified, in order to represent both the energy necessary to melt the entire load of aluminum, but also the possible heat losses inherent in the process. Since the liquid fuel superior heating power h_{ci} is 39.8 MJ/kg, the fuel mass flow rate was set as 108.5 kg/h. The diameter of the fuel droplets was defined as 0.1 μm, and their velocity magnitude was set as 10.5 m/s. The oxidant-fuel ratio was stoichiometrically defined, leading to an O_2 mass flow rate equal to 358 kg/h.

The O_2 mass fraction in the air is equal to 23%, therefore, for the second case, which employed air, the mass flow rate of air was defined as 1608 kg/h. However, for this case the amount of energy available for the aluminum fusion was significantly smaller than for the O_2 case, since it provided a heat transfer over the aluminum surface of 603 kW, and only 11 ton of melted aluminum could be obtained for the one hour period. To melt 16 tons, the duration of the process should be of least 1 hr and 28 minutes. This is probably due to the fact that an additional amount of energy is necessary to heat the nitrogen present in air, and also due to the large amount of nitrogen, a poor mixture of oxidant and fuel is obtained leading to a less efficient combustion.

To be able to compare the same process, a third case was analyzed, so that the same amount of melted aluminum in one hour could be obtained. The amount of fuel was increased so that a heat flux equal to 880 kW over the aluminum surface was obtained. The fuel mass flow rate was set as 180 kg/h (which corresponds to a 2.0 MW $C_{19}H_{30}$ flame), and the air mass flow rate was set as 2743 kg/h.

Since the oxidant was injected through three openings, the total amount of oxidant mass flow rate was equally divided into each inlet.

Due to space limitations and since the qualitative behavior of both air cases are similar, only the comparison between this last case and the oxygen case will be presented.

Temperature and heat flux distribution

Figures 2 to 7 present a comparison of the temperature and heat flux distribution inside the furnace, with the two types of oxidant. The purpose of the comparison is to identify the influence of the type of oxidant in the flame shape, temperature distribution and heat flux distribution over the load.

As already mentioned, the cases selected to be presented produced the same total heat transfer rate of 880 kW over the aluminum surface. Figure 2 shows an isosurface of 1600K, while Fig. 3 illustrates the temperature distribution through a y-z plane passing by the burners (x=0.8 m). The temperature distributions at the refractory wall are shown in Fig. 4. To better analyze the influence of the oxidants, Figs. 5 and 6 show temperature profiles along selected lines inside the furnace.

The flame shape for both oxidants can be appreciated by examining the 1600K isosurfaces (Fig. 2). Both flames follow the direction of the inlet jets, away from the refractory walls and downward into the load's surface. Figures 2a, 3a and 4a correspond to Case 1 (O_2) where a shorter and wider flame region can be seen, as well as higher temperatures. The combustion starts near the entrance, where high values are obtained, and then the temperature level rapidly drops below 1600K. The maximum temperature inside the furnace is 3403 K. The air results are presented in Figs. 2b, 3b and 4b. Due to the presence of the nitrogen, a very large amount of cold oxidant is injected. As a result the liquid droplet evaporation is delayed; the oxygen-fuel mixture is less efficient, and as it can be seen in Fig. 2b, the flame is detached from the inlet. The 1600K iso-surface is longer and higher temperatures are found near the back wall. For this case the maximum temperature inside the furnace is 1842 K.
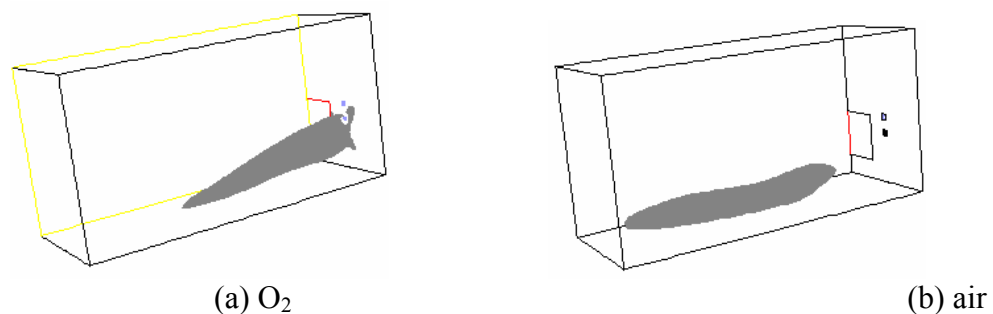

(a) O_2 (b) air

Figure 2. Isosurfaces of temperature, T=1600 K.

The O_2 flame is more intense and concentrated in the first half of the domain, leading to a less uniform temperature distribution on the lateral refractory walls (shown in Fig. 4) and could also compromise the uniformity of the heat flux on the aluminum surface (Fig. 7). At Figure 4, the influence of the flame at the refractory wall is clearly seen for the O_2 case, by the warm spots at the side wall (1469K). These warm spots can damage the refractory wall, increasing the cost of the project. Although warm spots were observed for the O_2 case, the average temperature at all the refractory walls are similar, around 1382K. Also, since the flame is shorter, the maximum wall temperature is observed at the frontal plane (1738K). Due to the longer flame, warm spots were also observed for the air case,(Fig 4b), but at the back wall and superior wall, reaching 1528 K and 1512 K, respectively. Although the flame temperature is smaller, the average wall temperature is equal to 1408 K, similar to the O_2 case, but slightly higher due to the hot spots at the superior and back walls.

(a) O$_2$ (b) air

T(K)   1300   1330   1360   1390   1420   1450

Figure 3 - Temperature distribution. Plane y-z (x=0.8 m)

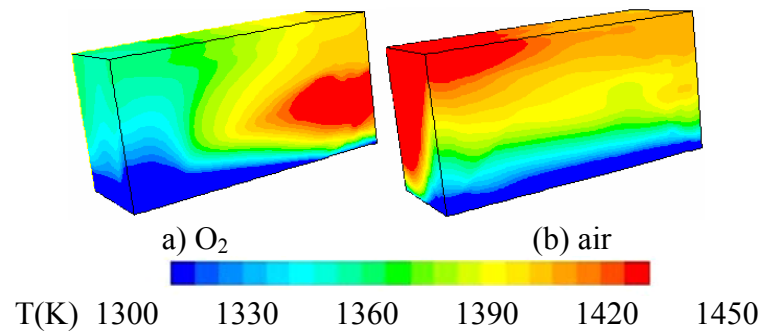a) O$_2$ (b) air

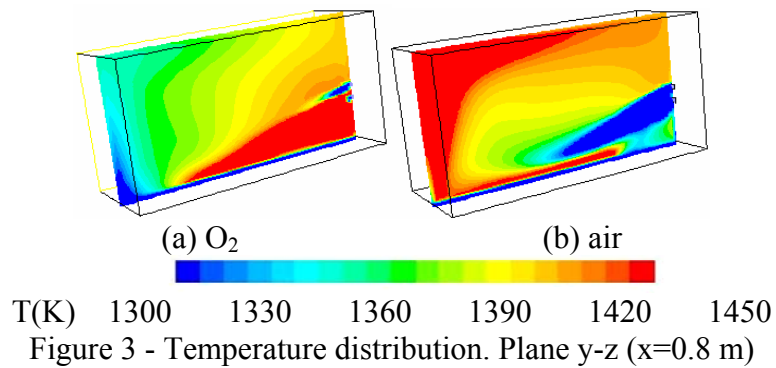T(K) 1300   1330   1360   1390   1420   1450

Figure 4 - Temperature distribution on the refractory walls.

By examining the temperature distribution on a plane that passes through the injectors (x = 0.80 m), it can be seen for the oxygen case (Fig 3a), the cold oxygen jet over the liquid fuel jet, close to the inlet region. Due to the combustion, a substantial temperature raise can be observed, under the cold jet. However, for the air case, due to high amount of nitrogen, the combustion is delayed, and the cold jet penetrates farther into the domain. The high temperatures due to the combustion can be seen close the aluminum surface, reaching the upper back part of the furnace. In spite of these differences, the temperature level inside the furnace is approximately the same for both oxidants (1410 K). However, it should be remembered that for the air case, a larger amount of liquid fuel was injected to reach the same level of heat flux at the load.

Figure 5 shows the temperature profile along the *z* coordinate for two lines inside the furnace. The first line (Fig. 5a) passes through the center of the burner (x = 0.80m and y = 0.65m), and the other one (Fig. 5b) passes through the center of the oxidant injector (x = 0.80m and y = 0.85m). It can be seen that, as already mentioned, the temperature levels inside the furnace is around 1410K for both oxidant. Figure 6 presents the temperature profile along the x direction, at the height of the burner, at two z positions near the entrance. There is a small depression on the temperature level at y=0.65 m and z=0.90 m (Fig. 6b), for both cases. This is due to the fact that the inlets fuel/oxygen are cold, and only after both species are brought to contact, the combustion process starts. Since there is only oxygen in the lower entrance, it reduces the temperature of the warmer mixture that arrives from the upper burner. Due to the high amount of nitrogen in the air stream, it is more difficult for the oxygen to mix with the C$_{19}$H$_{30}$, therefore, the reaction starts farther away from the entrance and lower temperatures can be seen at z = 0.25 m. The peak of temperature for the O$_2$ case indicates that the reaction had already started at that location.

The radiation heat flux on the aluminum surface is presented at Fig. 7. Due to the high temperature flame, the radiation heat flux is dominant. It can be seen large values of the radiation heat flux under the flame for both cases; however, since the O$_2$ flame was much more concentrated, a smaller high heat flux region can be seen near the entrance.
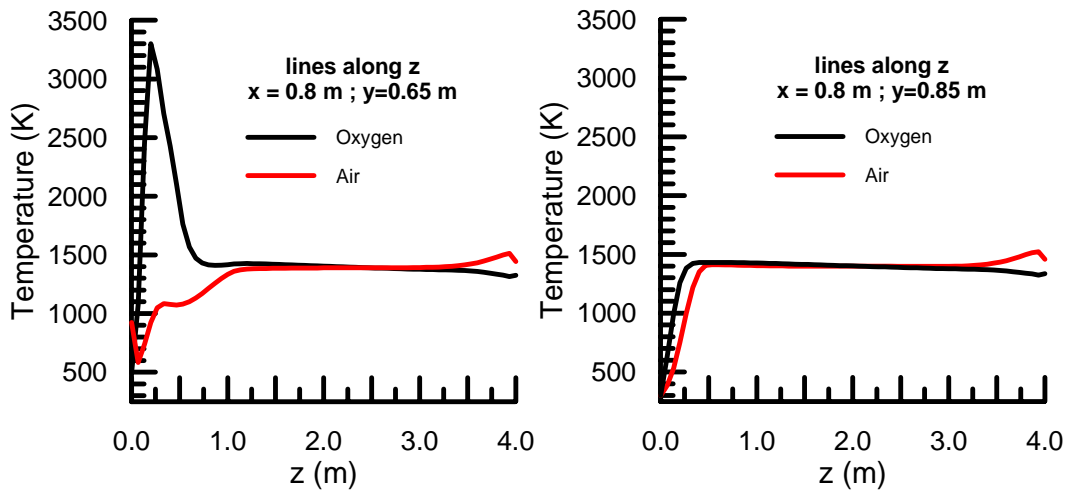
(a) x = 0.80 m; y = 0.65 m (b) x = 0.80 m; y = 0.85 m
Figure 5. Temperature profiles along z inside the furnace.
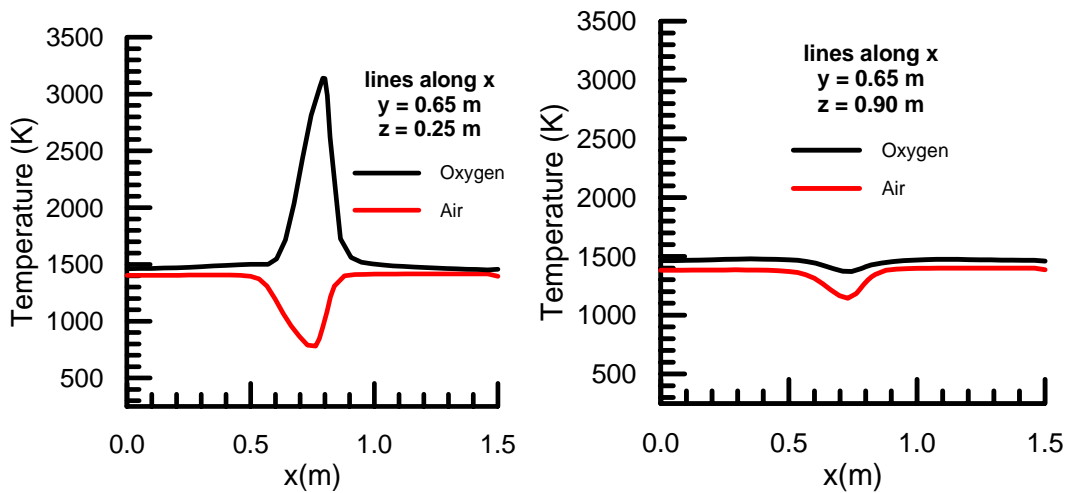
(a) y = 0.65 m; z = 0.25 m (b) y = 0.65 m; z = 0.90 m
Figure 6. Temperature profiles along x inside the furnace.
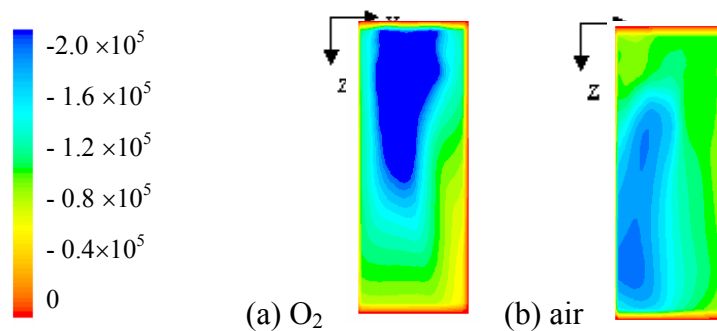

Figure 7. Distribution of radiation heat flux (W/m^2)

To help understand the flame displacement from the entrance, Fig. 8 illustrates the droplets trajectories, colored by their diameter size. For the air case, the evaporation occurs very close to the entrance, inducing the beginning of the combustion. For the air case, it can be seen in Fig. 8b, that the full evaporation only occurs at 1/4 of the furnace length, where the combustion begins.
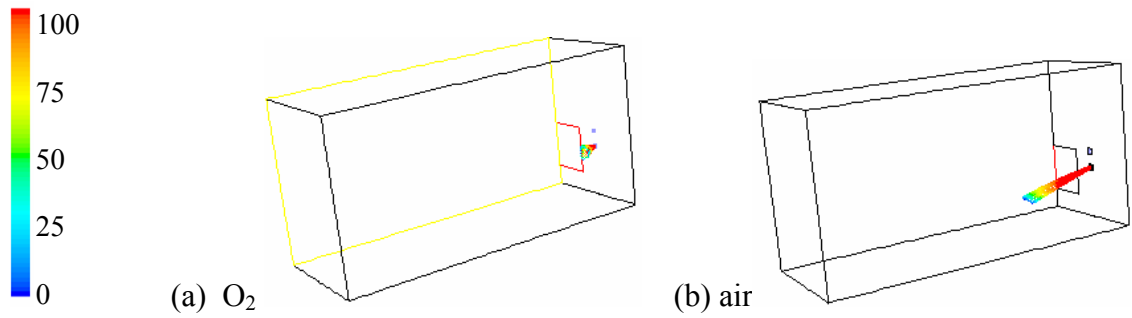
(a) O$_2$ (b) air

Figure 8. Particle tracking, colored by particle diameter (μm).

Species distribution

The analysis of the distribution of C$_{19}$H$_{30}$ gives a good idea of how the fuel is consumed inside the furnace. The fuel reacts with the oxygen to form the products. The reactants distributions also give a good idea of how the flame distributes itself along the furnace. The flame region is understood to be the region where the highest consumption of fuel occurs, followed by a great heat release and temperature raise. Comparison of the fuel and oxygen distributions for both cases are shown in Fig. 8, where iso-surfaces corresponding to 2% of mass fraction of C$_{19}$H$_{30}$ and 5% mass fraction of O$_2$ are presented. The mass concentrations of both species are higher inside the respective isosurfaces. It can be seen the O$_2$ isosurface connected with the upper and lower burner. The C$_{19}$H$_{30}$ is injected only at the lower burner; therefore the C$_{19}$H$_{30}$ concentration is high, below the O$_2$ jet. It can be observed that the reaction occurs near the entrance, for the O$_2$ case leading to low values of the reacting species in this region. It can be clearly seen that due to high amount of nitrogen present in the air, the O$_2$ distribution for this case is less concentrated, leading to a smaller 5% O$_2$ isosurface. Further, it can be noted a worse contact of the oxygen with the C$_{19}$H$_{30}$ at the gas phase, due to the presence of the nitrogen. As already mentioned, the combustion starts closer to the entrance for the O$_2$ case, leading to higher temperatures at that region, what can be seen by the red color. The blue indicates low temperatures, and it can be observed that while the droplets do not evaporate, there is no combustion and the inlet cold temperature is practically not altered.
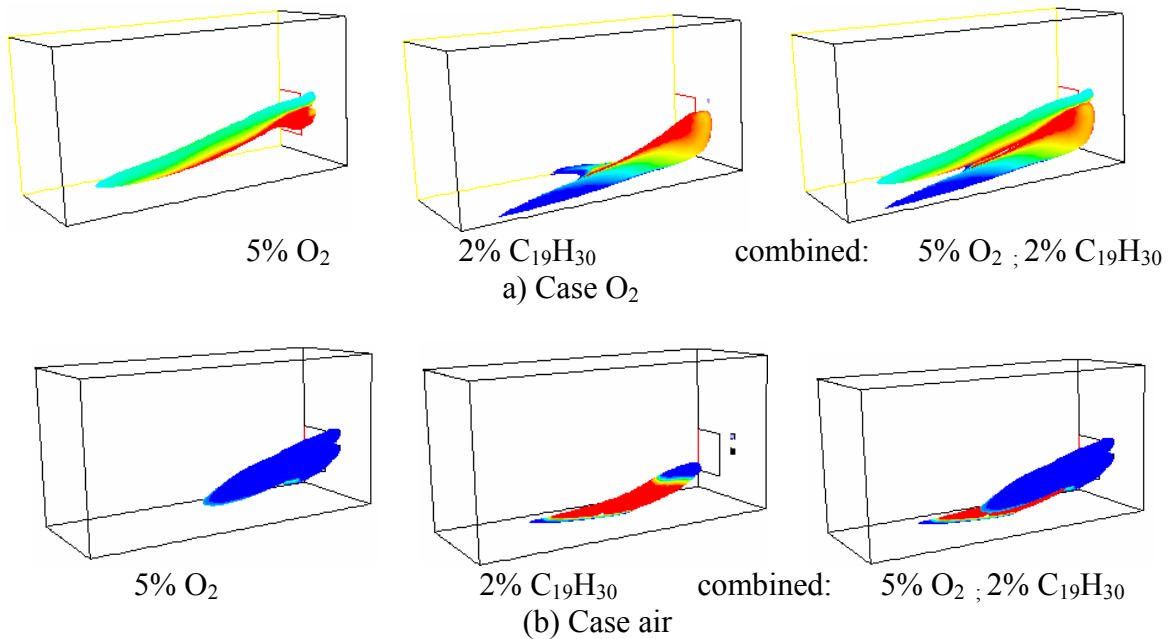

5% O$_2$ 2% C$_{19}$H$_{30}$ combined: 5% O$_2$; 2% C$_{19}$H$_{30}$

a) Case O$_2$

5% O$_2$ 2% C$_{19}$H$_{30}$ combined: 5% O$_2$; 2% C$_{19}$H$_{30}$

(b) Case air

Figure 9. Isosurfaces of 2% C$_{19}$H$_{30}$ and 5% O$_2$, colored by temperature.

The reaction of $C_{19}H_{30}$ with oxygen forms water and carbon dioxide. Figure 10 shows the CO_2 distribution at several *x-y* planes along the *z* axial coordinate, for both oxidants. It can be seen lower values in the flame region, since the products are still being formed. It can also be seen a smaller amount of CO_2 for the air case, which is a positive aspect related with the selection of this oxidant. For both cases, the concentration of CO_2 at the chimney is approximately uniform. The air case has a mass fraction concentration equal to 25% of the O_2 case concentration.
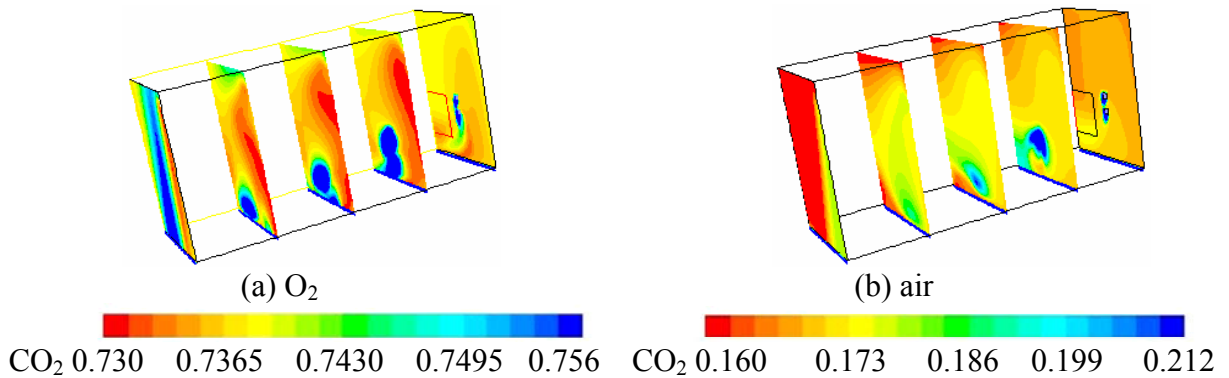

(a) O_2 (b) air

CO_2 0.730   0.7365   0.7430   0.7495   0.756 CO_2 0.160   0.173   0.186   0.199   0.212

Figure 10. Carbon Dioxide mass fraction inside the furnace. Planes x-y. z=0m, 1m, 2m, 3m and 4m.

Although the amount of CO_2 is smaller for the air case, a second type of pollutant is formed, which is the NOx. Its mass fraction distribution is illustrated at Fig. 11 at the plane that passes through the injectors (x = 0.80 m). It can be seen that, as expected, the NOx distribution follows the same profile of all other species at the x=0.8 m. Further, its concentration is approximately uniform at the chimney, and its average value is equal to 4.25 ppm. The presence of NOx is the worse inconvenient of employing air instead of pure oxygen.

Figure 12 shows the water distribution over the aluminum surface. High water concentration is not desirable because an aluminum oxide layer can be formed as water reacts with the surface of the load, which increases the thermal resistance and compromises the quality of the product. It is interesting to observe that the lowest water concentration is under the flame. Note however, that the water distribution is almost uniform in both cases. As with the CO_2 distribution, the air case produced smaller amount the water, which is also a desirable aspect, to avoid the aluminum oxidation.
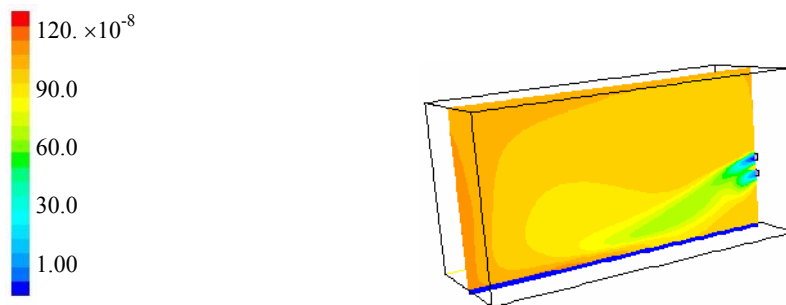

Figure 11. NOx mole mass fraction at plane y-z, x=0.8 m.
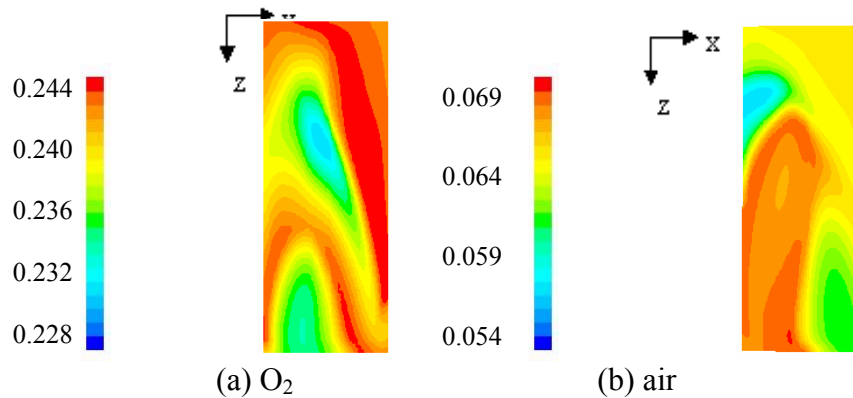
(a) O_2 (b) air

Figure 15. Water mass fraction distribution on the aluminum surface.

Conclusions

The numerical simulation of the process inside an aluminum melting furnace proved to be a helpful tool, which can contribute to improve several aspects of industrial interest, for example, reduction of material costs on maintenance of the refractory walls, increase of the efficiency of the fusion process, assurance of the quality of the product by the investigation of the deposition of water on the aluminum surface, better positioning of the burner and oxygen injectors, etc.

The numerical simulation also allows the easy investigation of the influence of several variables on the process; however, the mathematical models that will be used must be carefully chosen to maximize reliability on the results, not bringing unreal physical situations representing the phenomena.

The choice of the type of oxidant used as energy source for the aluminum fusion can be crucial to achieve better efficiency on the process. It was seen that the option for pure oxygen or air as oxidant can significantly alter the combustion aspects inside the furnace, such as the formation of too long or too intense flames, leading to hot spots on the refractory walls and a non uniform heat flux distribution on the aluminum load.

Although a direct numerical comparison with experimental results was not performed due to lack of experimental data, the turbulence and combustion models employed here were used to predict the flow characteristics in the industrial aluminum remelting reverb furnace (Nieckele et al., 2004) with reasonable results. Further, the flow field was obtained with the same model in a cylindrical furnace (Nieckele et al., 2001) and good agreement with experimental data was obtained.

The present analysis showed that the selection of air as oxidant has several advantages in relation to the use of pure oxygen. The temperature level inside the furnace is smaller, thus protecting the refractory walls, smaller products concentration were obtained at the chimney, and smaller water was found at the aluminum surface. However, in order to produce the same amount of melt aluminum, a larger amount of air had to be specified, reducing the advantage of employing a cheaper oxidant. Further, NOx was formed, in a non negligible amount.

References

Brewster, B.S.; Webb, B.W.; McQuay; M.Q.,D'Agostini, M. and Baukal, C.E., 2001, "Combustion measurements and modelling in an oxygen-enriched aluminium-recycling furnace," Journal of the Institute of Energy, 74, pp. 11-17.

Demoulin, F.X., Borghi, R., 2002, " Modeling of turbulent spray combustion with application to diesel like experiment", Combustion and Flame 129 (3), p. 281-293

Fenimore, C.P., 1971, "Formation of nitric oxide in premixed hydrocarbon flames", in 13th Int. Symp. on Combustion, p. 373, The Combustion Institute.

Frassoldati, A, Frigerio, S, Colombo, E, Inzoli, F, and Faravelli, T, 2005, "Determination of NOx emissions from strong swirling confined flames with an integrated CFD-based procedure", Chemical Engineering Science, v 60, pp 2851-2869.

Fluent User's Guide, v. 6.2, 2006, Fluent Inc., New Hampshire.

Hanson, R. K. and Salimian, S. 1984, "Survey of Rate Constants in H/N/O Systems". In W. C. Gardiner, editor, *Combustion Chemistry*, page 361.

Hill, SC, and Smoot, LD, 2000, "Modeling of nitrogen oxides formation and destruction in combustion systems", Progress in Energy and Combustion Science, v 26, pp 417-558

Kuo, K.K., 1986. Principles of Combustion, John Wiley & Sons, New York.

Launder, B.E. and Spalding, D.B., 1974. "The Numerical Computation of Turbulent Flows", Computer Methods in App. Mech. and Engineering, 3, p. 269-289.

Mukhopadhyay, A.; Puri, I.K.; Zelepouga, S. and Rue, D.M., 2001, "Numerical simulation of methane-air nozzle burners for aluminum remelt furnaces," *Proceedings of 2001 ASME-IMECE*, USA, CD-ROM, HTD-24234.

Nieckele, A.O., Naccache, M. F., Gomes, M. S. P., 2004, "Numerical Simulation of a Three Dimensional Aluminum Melting Furnace", Journal of Energy Resources Technology, ASME, vol. 126, pp.72-81.

Nieckele, A.O.; Naccache, M. F.; Gomes, M. S. P. and Kobayashi, W., 1999, "The influence of oxygen injection configuration in the performance of an aluminum melting furnace," Proceedings of 1999 ASME-IMECE, USA, Heat Transfer Division, **2**, pp. 405-412..

Nieckele, A.O.; Naccache, M.F.; Gomes, M. S. P.; Carneiro, J.N.E.; Serfaty, R., 2002, "Numerical simulation of natural gas combustion using a one step and a two step reaction", *Proceedings of 2002 ASME-IMECE*, November 11-16, New Orleans, LO, USA.

Nieckele, A.O.; Naccache, M.F., Gomes, M.S.P.; Carneiro, J.N.E.; Serfaty, R., 2001, "Models evaluations of combustion processes in a cylindrical furnace", *Procedings of 2001 ASME IMECE*, 2001, New York, NY, CD-ROM

Patankar, S.V. and Spalding, D.B., 1967. Heat and Mass transfer in Boundary Layers, Morgan-Grampian, London.

Reveillon, J.; Vervisch L.; 2000, "Spray vaporization in nonpremixed turbulent combustion modeling: a single droplet model", Journals of Combustion and Flame, April 2000, 121(1), pp. 75-90 (16).

Smith, T.F., Shen, Z.F., and Friedman, J.N., 1982. "Evaluation of Coefficients for the Weighted Sum of Gray Gases Model", Transactions of the ASME - Journal of Heat Transfer, v. 104, p. 602-608.

Soete, G.G., 1975, "Overall reaction rates of NO and N2 formation from fuel nitrogen", 15th Symp. on Combustion, p. 1093-1102, The Combustion Institute.

TECFLAM, 2006, German TECFLAM cooperation, page: www.tu-darmstadt.de/fb/mb/ekt/tecflam.

Tomeczek, J. and Gradón,B, 1997. "The Rate of Nitric Oxide Formation in Hydrocarbon Flames", Fourth International Conference on Technologies and Combustion for a Clean Environment, Lisbon , Portugal.

Wang, L, Haworth, DC, Turns, SR, and Modest, MF, 2005, "Interactions among soot, thermal radiation, and NOx emissions in oxygen-enriched turbulent non-premixed flames: a computational fluid dynamics modeling study", Combustion and Flame, v 141, pp 170-179.

Yang, WH, and Blasiak, W, 2005, "Numerical simulation of properties of a LPG flame with high-temperature air", International Journal of Thermal Sciences, v 44, pp 973-985.